PLASMA DYNAMICS

IV. PLASMAS AND CONTROLLED NUCLEAR FUSION

A. Waves and Radiation

Academic and Research Staff

Prof. G. Bekefi
Prof. W. P. Allis
Prof. A. Bers
Prof. S. C. Brown
Prof. B. Coppi
Prof. E. V. George
Prof. R. J. Taylor
Dr. P. A. Politzer
J. J. McCarthy
W. J. Mulligan

Graduate Students

F. W. Chambers
R. J. Hawryluk
D. O. Overskei
M. L. Vianna

1. CALCULATION OF SOME COUPLING COEFFICIENTS FOR THE INTERACTION OF TWO ELECTROMAGNETIC WAVES WITH AN ELECTROSTATIC WAVE IN A PLASMA

U. S. Atomic Energy Commission (Contract AT(11-1)-3070)

F. W. Chambers, R. J. Hawryluk, A. Bers

Introduction

Nonlinear wave-wave coupling, which has received considerable attention in recent years, is of particular interest at present in the development of laser fusion. As discussed by Rosenbluth and Sagdeev,[1] instabilities such as stimulated Brillouin and Raman scattering can determine the feasibility of several methods proposed to attain laser fusion. It is important not only to determine the threshold for the instability and its saturation mechanism but also to find out whether the instability is absolute or convective. Another proposal for nonlinear wave-wave coupling, which has been discussed by Bekefi,[2] is its use as a plasma diagnostic tool.

In order to design an experiment to verify the calculations for coupling coefficients and study the space-time development of the instability, the experimentalist must be familiar with the magnitude of the proposed effect and threshold conditions for the effect to be observed. We have evaluated a number of different coupling coefficients for two electromagnetic modes coupling to an electrostatic mode of a plasma. We have assumed throughout a coherent wave-wave interaction at resonance in an infinite homogeneous medium without density gradients, as discussed by Bers,[3] whose formalism is employed in this report. A second-order current resulting from the presence of the two electromagnetic modes is calculated. The time rate of change of the electrostatic mode amplitude is determined from this second-order current, which acts to drive the mode. The coupling coefficient thus derived can be used to relate the changes of amplitude of any

one mode to the amplitudes of the other two modes. In this report we do not derive the coupling of modes theory but only describe the pertinent equations.

Theory

We shall discuss only 3 wave interactions. The mode-coupling equations are

$$\left(\frac{\partial}{\partial t} + \vec{v}_{g1} \cdot \nabla + \gamma_1\right) a_1 = p_1 K a_2 a_3 \tag{1}$$

$$\left(\frac{\partial}{\partial t} + \vec{v}_{g2} \cdot \nabla + \gamma_2\right) a_2 = -p_2 K^* a_1 a_3^* \tag{2}$$

$$\left(\frac{\partial}{\partial t} + \vec{v}_{g3} \cdot \nabla + \gamma_3\right) a_3 = -p_3 K^* a_1 a_2^*. \tag{3}$$

These equations couple three modes at $(\omega_1, \vec{k}_1)$, $(\omega_2, \vec{k}_2)$ and $(\omega_3, \vec{k}_3)$, where we assume that modes 1 and 2 are electromagnetic, with ω_1 as the higher frequency. Furthermore, we assume that the resonance conditions are satisfied exactly:

$$\vec{k}_3 = \vec{k}_1 - \vec{k}_2 \tag{4}$$

$$\omega_3 = \omega_1 - \omega_2. \tag{5}$$

We allow for a weak phenomenological damping by including γ_n in the coupling equations. We define a_n by

$$|a_n(\vec{r}, t)|^2 = \frac{\epsilon_0}{4} \left|\frac{\partial D_n}{\partial \omega}\right| E_n^2 \tag{6}$$

$$\vec{E}_n = \vec{e}_n E_n; \qquad |\vec{e}_n|^2 = 1; \qquad E_n \text{ real}, \tag{7}$$

where $\vec{e}_n$ is the complex polarization vector. D_n is defined in terms of the general dispersion tensor $\overline{\overline{D}}$.

$$D_n(\vec{k}, \omega) = \vec{e}_n^* \cdot \overline{\overline{D}}(\vec{k}, \omega) \cdot \vec{e}_n. \tag{8}$$

The parity or the sign of the mode energy, p_n is defined as

$$p_n = \frac{\partial D_n}{\partial \omega} \Big/ \left|\frac{\partial D_n}{\partial \omega}\right|. \tag{9}$$

The coupling coefficient is given by

$$K = \frac{-1}{4\omega_3} \frac{\vec{e}_3 \cdot \vec{J}_2^3}{E_1 E_2 \left(\frac{\epsilon_o}{4}\right)^{3/2} \left| \frac{\partial D_1}{\partial \omega} \frac{\partial D_2}{\partial \omega} \frac{\partial D_3}{\partial \omega} \right|^{1/2}}. \tag{10}$$

$\vec{J}_2^3$ is the second-order nonlinear current at $\omega_3, \vec{k}_3$ which drives the interaction. Note that we are considering only nonlinear interactions where momentum and energy are conserved; thus, the same K appears in all three equations. $\vec{J}_2^3$ for modes 1 and 2 transverse ($\vec{k} \cdot \vec{E} = 0$) is given by[3]

$$\frac{\vec{J}_2^3}{E_1 E_2} = \frac{1}{2n_o q} \left(\vec{e}_2^* \cdot \overline{\overline{\sigma}}_1 \cdot \vec{e}_1\right) \overline{\overline{\sigma}}_3 \cdot \frac{\vec{k}_2}{\omega_2} - \frac{1}{2n_o q} \left(\frac{\vec{k}_2}{\omega_2} \cdot \overline{\overline{\sigma}}_1 \cdot \vec{e}_1\right) \overline{\overline{\sigma}}_3 \cdot \vec{e}_2^*$$

$$- \frac{im}{2n_o^2 q^3} \left(-\vec{k}_2 \cdot \overline{\overline{\sigma}}_1 \cdot \vec{e}_1\right) \overline{\overline{\sigma}}_3 \cdot \left(\overline{\overline{\sigma}}_2^* \cdot \vec{e}_2^*\right) + (1 \rightleftharpoons 2^*), \tag{11}$$

where $\overline{\overline{\sigma}}_n$ is the first-order conductivity at $\omega_n, \vec{k}_n$, as derived from the fluid model. For electromagnetic waves with $\omega \gg \omega_{ce}$ we can assume a scalar conductivity that simplifies Eq. 11, since the second and third terms cancel. The resultant second-order electron current, properly symmetrized is

$$\frac{\vec{J}_2^3}{E_1 E_2} = \frac{-iq}{2m_e \omega_1 \omega_2} \overline{\overline{\sigma}}_3 \cdot \vec{k}_3 \left(\vec{e}_1 \cdot \vec{e}_2^*\right). \tag{12}$$

Calculation of Coupling Coefficients

a. EM/EM/EP Coupling

In this coupling, two electromagnetic waves propagating at an angle ϕ, whose polarization vectors are at an angle α ($\alpha \neq \phi$), interact to produce an electron-plasma oscillation. The angles are delineated in Fig. IV-1; note that a magnetic field has been included, although for this coupling we assume $\vec{B}_o = 0$, $k\lambda_D \ll 1$, and ignore the ion contribution to the plasma oscillation. With these approximations,

$$\omega_3^2 = \omega_{pe}^2 + 3k^2 v_{Te}^2 \approx \omega_{pe}^2 \tag{13}$$

$$K = \frac{|q|}{(\epsilon_o)^{1/2}} \left(\frac{k_3 \cos \alpha}{m_e \omega_1 \omega_2}\right) \left(\frac{\omega_1 \omega_2 \omega_{pe}}{8}\right)^{1/2}. \tag{14}$$

Two cases are of special interest.

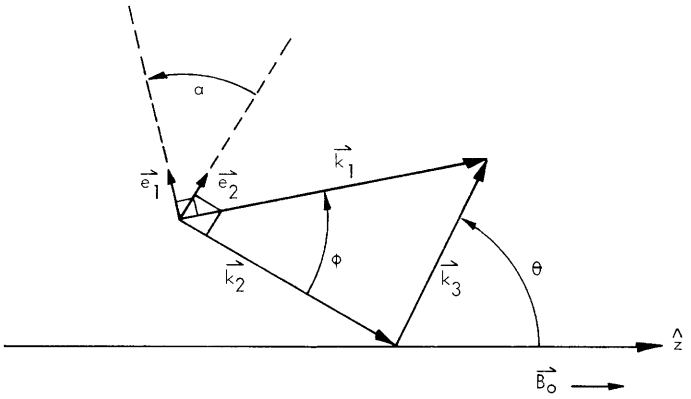

Fig. IV-1. Diagram of wave vectors and angles for three-wave couplings.

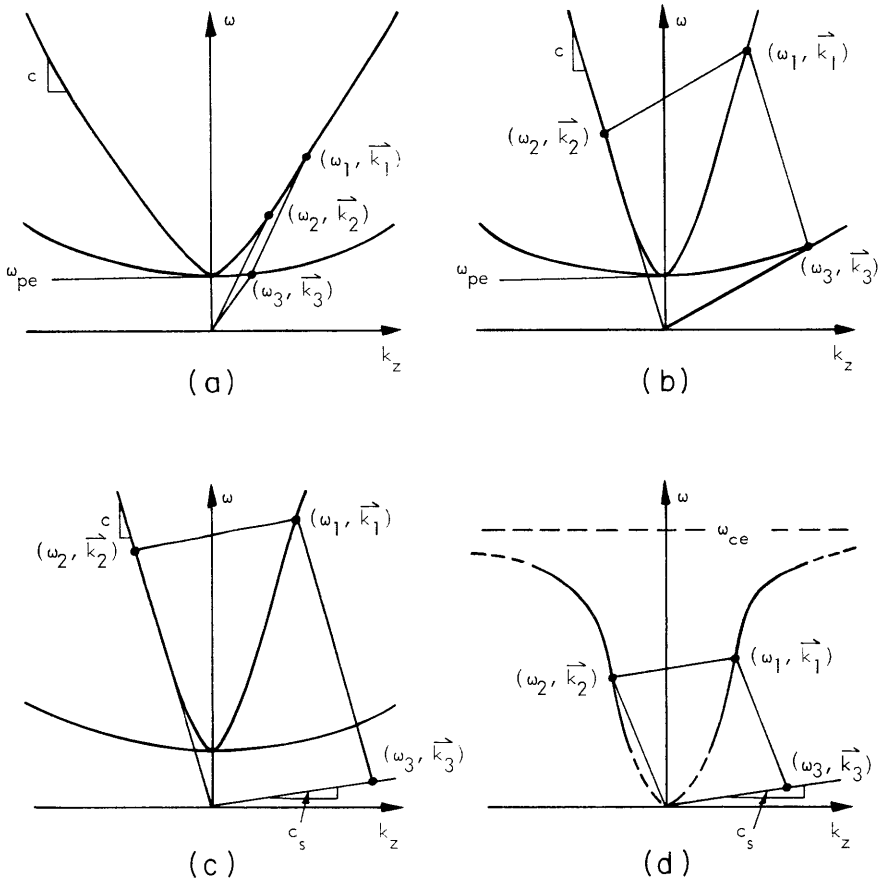

Fig. IV-2. Dispersion-relation diagrams for several collinear three-wave couplings (not to scale).
(a) Raman forward scattering.
(b) Raman backward scattering.
(c) Brillouin backward scattering.
(d) Whistler backward scattering.

Forward Scattering ($\phi = 0°$) (Fig. IV-2a).

If $\omega_{1,2} \gg \omega_{pe}$, then $\omega_{pe} = ck_3 = c(k_1 - k_2)$.

$$K = \frac{|q|}{(\epsilon_o)^{1/2}} \left(\frac{\omega_{pe} \cos \alpha}{m_e c \omega_1 \omega_2}\right) \left(\frac{\omega_1 \omega_2 \omega_{pe}}{8}\right)^{1/2} . \tag{15}$$

Backward Scattering ($\phi = 180°$) (Fig. IV-2b).

If $\omega_{1,2} \gg \omega_{pe}$, then $k_3 = \frac{\omega_1 + \omega_2}{c} \approx \frac{2\omega_1}{c}$.

$$K = \frac{|q|}{(\epsilon_o)^{1/2}} \left(\frac{2 \cos \alpha}{m_e c \omega_2}\right) \left(\frac{\omega_1 \omega_2 \omega_{pe}}{8}\right)^{1/2} . \tag{16}$$

b. EM/EM/IA Coupling

This coupling is similar to EM/EM/EP, except that the electrostatic mode is an ion-acoustic wave. We shall consider a magnetic field in the +z direction and include the effects of $v_{Te} \neq 0$. We assume $\omega_{1,2} \gg \omega_{pe}, \omega_{ce}$ so that the electromagnetic waves are unaffected by the plasma or the magnetic field. The ion-acoustic wave will propagate at an angle θ with respect to the magnetic field (see Fig. IV-1). Under the conditions when an acoustic wave will propagate we obtain

$$\omega_3 = c_s k_3 \qquad c_s^2 = \frac{K_B T_e}{m_i} \tag{17}$$

$$K = -\frac{|q|}{(\epsilon_o)^{1/2}} \left(\frac{\omega_{pe}^2 \cos \alpha \, k_3}{m_i \omega_1 \omega_2 \omega_3^2}\right) \left(\frac{\omega_1 \omega_2 \omega_3^3}{8\omega_{pi}^2}\right)^{1/2} . \tag{18}$$

Backward Scattering ($\phi = 180°$) is an especially interesting case for some plasmas. If the two electromagnetic waves are moving in opposite directions, as illustrated in Fig. IV-2c, then

$$k_3 = 2k_1 = \frac{2\omega_1}{c}$$

$$K = -\frac{|q|}{(\epsilon_o)^{1/2}} \left(\frac{2\omega_{pe}^2 \cos \alpha}{m_i \omega_2 \omega_3^2 c}\right) \left(\frac{\omega_1 \omega_2 \omega_3^3}{8\omega_{pi}^2}\right)^{1/2} . \tag{19}$$

c. EM/EM/LH Coupling

This calculation is very similar to that for ion-acoustic waves. The lower hybrid mode exists in a magnetized plasma for a very small spectrum of angles nearly perpendicular to the magnetic field, namely $\cos^2\theta < m_e/m_i$. Since the lower hybrid mode is a cold-plasma mode, we assume for simplicity that $v_{Te} = v_{Ti} = 0$. The dispersion relation for $\omega_3 \gg \omega_{ci}$ is

$$\omega_3^2 = \frac{\omega_{pi}^2 + \omega_{pe}^2 \cos^2\theta}{1 + \omega_{pe}^2/\omega_{ce}^2} \tag{20}$$

$$K = -\frac{|q|}{(\epsilon_o)^{1/2}} \left(\frac{k_3 \omega_{pe}^2 \cos\alpha \left(1 - \cos^2\theta\, \omega_{ce}^2/\omega_3^2\right)}{m_e \omega_1 \omega_2 \omega_{ce}^2} \right) \left(\frac{\omega_1 \omega_2 \omega_3^3}{8\left(\omega_{pe}^2 \cos^2\theta + \omega_{pi}^2\right)} \right)^{1/2} . \tag{21}$$

d. EM/EM/UH Coupling

We may also couple to the upper hybrid mode, a cold-plasma mode propagating perpendicular to the static magnetic field ($\theta = 90°$). The dispersion relation and coupling coefficient are

$$\omega_3^2 = \omega_{ce}^2 + \omega_{pe}^2 \tag{22}$$

$$K = \frac{|q|}{(\epsilon_o)^{1/2}} \left(\frac{k_3 \cos\alpha}{m_e \omega_1 \omega_2} \right) \left(\frac{\omega_1 \omega_2 \omega_{pe}^2}{8\omega_3} \right)^{1/2} . \tag{23}$$

e. WH/WH/IA Coupling

This coupling is different from the others, in that the free-space electromagnetic waves are replaced by the whistler modes of a magnetized plasma. This allows us to propagate a wave into the plasma at well below the plasma frequency and thereby couple relatively more power into the ion-acoustic wave. The whistler mode is transverse ($\vec{k} \cdot \vec{E} = 0$); it is circularly polarized and the electric field rotates in the same sense that electrons gyrate around the magnetic field. In calculating the second-order nonlinear current we can no longer assume a scalar conductivity for $\bar{\bar{\sigma}}_{1,2}$; we must use Eq. 11. We shall consider only the case in which the whistler modes propagate in opposite directions along the magnetic field, as illustrated in

Fig. IV-2d. The dispersion relation is

$$\omega = \frac{|\omega_{ce}| c^2 k^2}{\omega_{pe}^2}. \tag{24}$$

Under the assumption that $\omega_1 \approx \omega_2$, the coupling coefficient is

$$K = -\frac{|q|}{(\epsilon_o)^{1/2}} \left(\frac{\omega_{pe}^2 k_3}{m_i \omega_2 |\omega_{ce}| \omega_3^2} \right) \left(\frac{\omega_{ce}^2 \omega_1^2 \omega_2^2 \omega_3}{2\omega_{pe}^4 \omega_{pi}^2} \right)^{1/2}. \tag{25}$$

Thresholds and Coupling Amplitudes

We shall now examine two experimental situations. The first is the two-pump case in which we can calculate the amplitude of the third wave produced by the nonlinear interaction. We shall consider as pumps only the two undamped electromagnetic waves. Then we shall consider the one-pump case, in which we shall calculate the threshold for instability in time, assuming spatial uniformity.

a. Two-Pump Case

Let us assume that a_1 and a_2 are externally driven so that their amplitude variations arising from nonlinear effects can be ignored. Then the nonlinear coupling equation can be written

$$\left(\frac{\partial}{\partial t} + \gamma_3 \right) a_3 = -p_3 K^* a_{10} a_{20}^*, \tag{26}$$

whose solution is

$$a_3 = \frac{-p_3 K^* a_{10} a_{20}^*}{\gamma_3} \left\{ 1 - e^{-\gamma_3 t} \right\}. \tag{27}$$

We evaluate the fluctuating potential of the electrostatic wave, $\tilde{\phi}_3$, in the limit $\gamma_3 t \gg 1$ which occurs when the amplitude has saturated. In the electrostatic case, the fluctuating potential can simply be related to the electric field of the wave, which in turn can be related to the normalized amplitude of the wave,

$$|\tilde{\phi}_3| = \left| \frac{E_3}{k_3} \right| = \frac{1}{\left(\frac{\epsilon_o}{4} \left| \frac{\partial D_3}{\partial \omega} \right| \right)^{1/2}} \frac{|K^* a_{10} a_{20}^*|}{\gamma_3}. \tag{28}$$

Table IV-1 is a listing of the fluctuating potentials that could be measured experimentally for the various interactions. Note that all of these calculations are subject to the approximations that we have used in deriving the coupling coefficients, as well as the assumption, inherent in our approach, of an infinite homogeneous medium without density gradients.

b. One-Pump Case

Let us consider that only one electromagnetic wave, whose amplitude is constant and unaffected by the nonlinear interaction, is being driven externally. Furthermore, let us

Table IV-1. Two-pump fluctuating potential. $V_n \triangleq \frac{qE_n}{m_e \omega_n}$.

EM + EM → EP

$$|\tilde{\phi}_3| = \frac{1}{4} V_1 V_2 \left(\frac{\omega_{pe}}{\gamma_3}\right)\left(\frac{m_e}{q}\right) \cos \alpha$$

EM + EM → IA

$$|\tilde{\phi}_3| = \frac{1}{4} V_1 V_2 \left(\frac{\omega_3}{\gamma_3}\right)\left(\frac{m_e}{q}\right) \cos \alpha$$

EM + EM → LH

$$|\tilde{\phi}_3| = \frac{1}{4} V_1 V_2 \left(\frac{\omega_3}{\gamma_3}\right)\left(\frac{\omega_3^2}{\omega_{ce}^2}\right)\left(\frac{\omega_{pe}^2 - \frac{\omega_{pe}^2}{\omega_3^2}\omega_{ce}^2 \cos^2\theta}{\omega_{pe}^2 \cos^2\theta + \omega_{pi}^2}\right)\left(\frac{m_e}{q}\right) \cos \alpha$$

EM + EM → UH

$$|\tilde{\phi}_3| = \frac{1}{4} V_1 V_2 \left(\frac{\omega_{pe}^2}{\omega_3 \gamma_3}\right)\left(\frac{m_e}{q}\right) \cos \alpha$$

WH + WH → IA

$$|\tilde{\phi}_3| = \frac{1}{4} V_1 V_2 \left(\frac{\omega_1 \omega_3}{|\omega_{ce}| \gamma_3}\right)\left(\frac{m_e}{q}\right)$$

Table IV-2. Temporal thresholds.

EM → EM + EP

$$\frac{V_1^2}{c^2} > 16\left(\frac{\gamma_2}{\omega_2}\right)\left(\frac{\gamma_3}{\omega_{pe}}\right)\frac{k_2^2}{k_3^2}\frac{1}{\cos^2\alpha}$$

EM → EM + IA

$$\frac{V_1^2}{v_{Te}^2} > 16\left(\frac{\gamma_2}{\omega_2}\right)\left(\frac{\gamma_3}{\omega_3}\right)\frac{\omega_2^2}{\omega_{pe}^2}\frac{1}{\cos^2\alpha}$$

EM → EM + LH

$$\frac{V_1^2}{c^2} > 16\left(\frac{\gamma_2}{\omega_2}\right)\left(\frac{\gamma_3}{\omega_3}\right)\frac{m_e}{m_i}\frac{\omega_{ce}^4}{\omega_{pe}^2\omega_3^2}\frac{k_2^2}{k_3^2}\frac{1}{\cos^2\alpha}\frac{\left(\frac{m_i}{m_e}\cos^2\theta + 1\right)}{\left(1 - \frac{\omega_{ce}^2}{\omega_3^2}\cos^2\theta\right)^2}$$

EM → EM + UH

$$\frac{V_1^2}{c^2} > 16\left(\frac{\gamma_2}{\omega_2}\right)\left(\frac{\gamma_3}{\omega_3}\right)\frac{\omega_3^2}{\omega_{pe}^2}\frac{k_2^2}{k_3^2}\frac{1}{\cos^2\alpha}$$

WH → WH + IA

$$\frac{V_1^2}{v_{Te}^2} > 8\left(\frac{\gamma_2}{\omega_2}\right)\left(\frac{\gamma_3}{\omega_3}\right)\frac{\omega_2|\omega_{ce}|}{\omega_1^2}$$

consider the coupling only in time and ignore all finite boundaries, as we have done throughout this report. The coupling equations are

$$\left(\frac{\partial}{\partial t} + \gamma_2\right) a_2 = -p_2 K^* a_{10} a_3^*, \tag{29}$$

$$\left(\frac{\partial}{\partial t} + \gamma_3\right) a_3 = -p_3 K^* a_{10} a_2^*. \tag{30}$$

Assuming solutions of the form

$$a_2 = A_2 \exp(-ist) \tag{31}$$

$$a_3 = A_3 \exp(is^* t), \tag{32}$$

we arrive at the threshold condition for growth in time,

$$|a_{10}|^2 > p_2 p_3 \frac{\gamma_2 \gamma_3}{|K|^2}. \tag{33}$$

Note that $p_2 = p_3 = +1$, corresponding to positive energy modes, is a necessary condition for the growth of an instability. In many physical situations of interest even more stringent conditions must be met, depending on the boundary conditions and the initial conditions of the system. We shall not elaborate on this extremely important point. The temporal thresholds for the interactions studied are tabulated in Table IV-2.

Conclusion

On the basis of this analysis we conclude that two-pump experiments either with high-power lasers or strong microwave sources are feasible. Indeed, recently several two-microwave pump couplings have been observed;[4] these are dominated, however, by finite geometry effects. One-pump experiments, on the other hand, are far more difficult, although instabilities can be excited by the very large glass lasers now available. When deciding which experiments are actually feasible, the experimenter must consider carefully not only the magnitudes of the coupling coefficients calculated in this report but also the exact effects of finite geometries and spatial and temporal nonuniformities in the plasma and pumps.

References

1. M. N. Rosenbluth and R. Z. Sagdeev, in Comments on Plasma Physics and Controlled Fusion, Vol. 1, No. 4, pp. 129-136, July-August 1972.

2. G. Bekefi, "Advances in Plasma Diagnostics with Waves and Radiation," in P. A. Davenport (Ed.), Tenth International Conference on Phenomena in Ionized Gases 1971 (Donald Parson and Co., Ltd, Oxford, England), pp. 299-332.

3. A. Bers, Notes on Lectures: Linear Waves and Instabilities, given at Ecole d'Eté de Physique Théorique, Les Houches, France (Gordon and Breach, New York, in press).

4. D. Phelps, N. Rynn, and G. Van Hoven, Phys. Rev. Letters 26, 688-691 (1971).

2. EFFECT OF PLASMA TURBULENCE UPON AN OPTICAL TRANSITION HAVING A NEARBY FORBIDDEN COMPONENT

U. S. Atomic Energy Commission (Contract AT(11-1)-3070)

G. Bekefi, C. Deutsch

[Dr. C. Deutsch is at the Laboratoire de Physique de Plasma, Faculté des Sciences, Orsay, France, where part of this work was carried out.]

In plasmas, turbulent electric field fluctuations are known to exist with intensities ranging from thousands of volts per centimeter to hundreds of kilovolts per centimeter. When such fields act on radiating atoms (or ions), they cause a variety of interesting phenomena[1] associated with the Stark splitting of energy states. Indeed, the resulting changes in the observed optical spectra are being used as a means of diagnosing the properties of the turbulence.

In this report we compute the line shape of the 2^3P-4^3D line of He I at 4471.48 Å and of its companion forbidden line, 2^3P-4^3F at 4470.04 Å. For purposes of this preliminary study we make the following assumptions.

(i) The plasma is very turbulent, but has such low charge density that classical collisions can be neglected. In other words, the Holtsmark field of the ions is taken to be small compared with the turbulent field. Similarly, electron impact broadening is omitted.

(ii) The turbulence is of low frequency and is assumed to be quasi-static; it is spatially homogeneous and isotropic. Such fully developed turbulence is expected to have the "normal" three-dimensional Gaussian distribution,

$$W(E)\,dE = 4\pi\left[\frac{1}{2\pi\sigma}\right]^{3/2} E^2\, e^{-E^2/2\sigma}\, dE, \tag{1}$$

with E as the magnitude of the electric field. The normalization is such that

$$\int_0^\infty W(E)\,dE = 1. \tag{2}$$

The quantity σ is the standard deviation and is connected to the mean-square electric field through the relation

$$\langle E^2 \rangle = \int_0^\infty E^2 W(E)\, dE = 3\sigma.$$

Computations of the line shape now follow standard procedure.[2] Figure IV-3 shows the intensity I(λ) for three different values of electric field strength. The

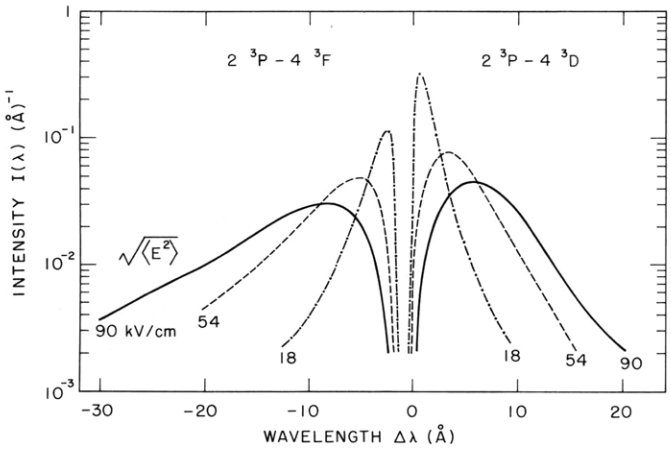

Fig. IV-3.
Line profiles of the He I 2^3P-4^3D allowed line at 4471.48 Å, and of the 2^3P-4^3F forbidden component. Three different values of the Gaussian-distributed electric field are considered. The wavelength $\Delta\lambda = 0$ on the abscissa corresponds to the wavelength position of the unperturbed allowed line.

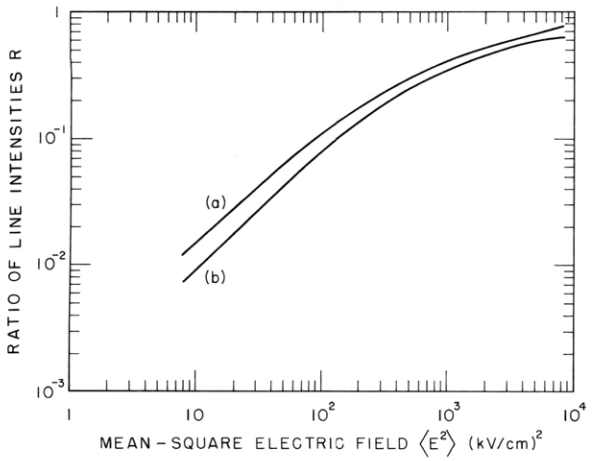

Fig. IV-4.
Ratio of forbidden to allowed intensities as a function of the mean-square Gaussian field. Curve (a) refers to integrated intensities and curve (b) refers to peak intensities.

total area under the combined allowed plus forbidden lines is normalized in each case so that

$$\int_0^\infty I(\lambda)\, d\lambda = 1. \tag{3}$$

A comparison of the line shapes with those derived by Griem[2] for the classical thermal plasma obeying the Holtsmark distribution shows marked differences. Thus the presence of strong turbulence in the plasma should be easily discernible. The magnitude

of the turbulent electric field can then be obtained by fitting the experimental and theoretical profiles.

In Fig. IV-4 we plot as a function of $\langle E^2 \rangle$ the ratio R of forbidden (F) to allowed (A) line intensities. The curve marked (a) refers to the ratio of integrated line intensities, namely

$$R = \frac{\int I_F(\lambda)\, d\lambda}{\int I_A(\lambda)\, d\lambda}. \tag{4}$$

On the other hand, the curve marked (b) denotes the ratio of the peak intensities of the respective lines. We note that at low fields the ratio of the integrated line intensities varies approximately as $\langle E^2 \rangle$, in accord with expectations. At high electric fields, however, R is more nearly linearly proportional to the electric field.

We plan to make line-shape calculations for one-dimensional turbulence [where W(E) is a one-dimensional Gaussian and is thus peaked at the origin E = 0]. The inclusion of electron impact broadening is being considered.

References

1. G. Bekefi, in Comments on Plasma Physics and Controlled Fusion, Vol. I, No. 1, pp. 9-16, January-February 1972.
2. H. R. Griem, Astrophys. J. 154, 1111 (1968).